Defects in interfacial layers and their role in the growth of ZnO nanorods by metallorganic chemical vapor deposition

Dong Jun Park and Jeong Yong Lee
Department of Materials Science and Engineering, Korea Advanced Institute of Science and Technology, 373-1 Guseong-dong, Yuseong-gu, Daejeon 305-701, Korea

Dong Chan Kim, Sanjay Kumar Mohanta, and Hyung Koun Cho[a)]
School of Advanced Materials Science and Engineering, Sungkyunkwan University, 300 Cheoncheon-dong, Jangan-gu, Suwon, Gyeonggi-do 440-746, Korea

(Received 9 July 2007; accepted 16 September 2007; published online 3 October 2007)

We report the evolution of ZnO nanorods by metalorganic chemical vapor deposition on sapphire substrates and an investigation of their microstructure. Well-aligned ZnO nanorods with a high aspect ratio were grown on an interfacial layer with several types of defects at a lower reactor pressure. Planar defects such as stacking mismatch boundaries and inversion domain boundaries were formed in the interfacial layer during the coalescence of the islands, and finally constituted the side facets of the nanorods. Based on the microstructural changes and origin of the defects in the interfacial layers, we propose a model to explain the growth evolution of ZnO nanorods on sapphire substrates. © *2007 American Institute of Physics*. [DOI: 10.1063/1.2794418]

One-dimensional (1D) semiconducting oxide nanomaterials have attracted much attention because of their interesting optical, electrical, and magnetic properties which are distinctive from those of the conventional bulk materials.[1,2] In particular, ZnO nanorods having a direct band gap of 3.37 eV and an exciton binding energy of 60 meV have the potential to be used in practical applications in nanoscale laser diodes, sensors, varistors, and so on.[3–5] Moreover, well-aligned nanorods grown directly on the substrates without the assistance of a metal catalyst are required for many applications of ZnO nanorods in various areas. With regard to this, metalorganic chemical vapor deposition (MOCVD) has been demonstrated to be a promising tool for the synthesis of vertically well-aligned nanorods with uniform length and thickness.[6,7] Although a lot of work has been reported on the catalyst-free growth of ZnO nanorods using MOCVD, their nanostructure growth evolution is not yet satisfactorily understood. In this letter, we report our attempt to explain the growth mechanism of MOCVD grown ZnO nanorods by taking into consideration their morphological and microstructural changes under different reactor pressures. In the heteroepitaxy growth of GaN and ZnO thin films having a wurtzite structure, the representative defects are threading dislocations (TDs) and planar defects (PDs) such as inversion domain boundaries (IDBs) and stacking mismatch boundaries (SMBs).[8,9] We believe these defects have a huge impact on the evolution of the ZnO nanorods. Based on the microstructural changes and origin of the defects in the interfacial layers, we propose a model to explain the growth mechanism of ZnO nanorods on sapphire substrates.

1D ZnO nanorods were grown on sapphire substrates using a MOCVD system with a vertical cold-wall reactor. The growth of the ZnO nanorods was performed at 380 °C for 30 min under different reactor pressures of 1, 3, and 5 Torr. Diethylzinc and pure oxygen gas were used as precursors. The flow rates of argon carrier gas and reactive oxygen gas were set to 10 and 50 SCCM (standard cubic centimeter per minute), respectively. The morphology of the ZnO nanorods was investigated by field emission scanning electron microscopy (FE-SEM) (JSM6700F) and transmission electron microscopy (TEM) (JEM 3010) operated at 300 kV.

Figure 1 shows the morphology and microstructural evolutions of the ZnO layers deposited at different reactor pressures of 1 (sample A), 3 (sample B), and 5 Torr (sample C). Sample A showed vertically well-aligned nanorods with sharp tips and a high aspect ratio, which exhibited a uniform distribution with mean diameters and lengths of ~71 nm and 1.4 μm, respectively [Fig. 1(a)]. However, the nanorods become shorter and fatter when the reactor pressure was increased to 3 Torr [Fig. 1(b)], and at 5 Torr a ZnO thin film with a rugged surface morphology was observed [Fig. 1(c)]. The insets of Figs. 1(a) and 1(c) represent the top view FE-SEM images of the ZnO layers grown for the short time of 60 s under reactor pressures of 1 and 5 Torr, respectively. Islands with increased diameters having a random size distribution were observed at a high reactor pressure, while the

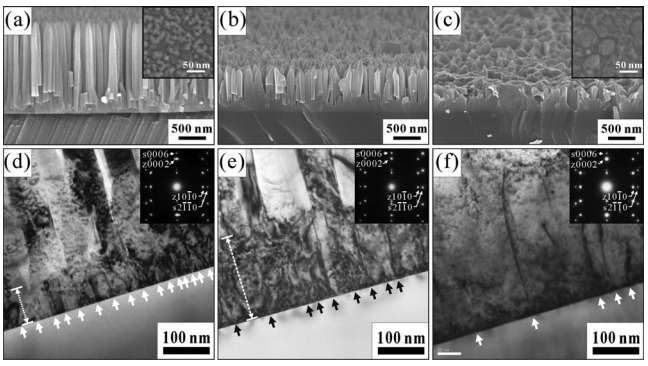

FIG. 1. [(a), (b), and (c)] Tilted-view SEM and [(d), (e), and (f)] cross-sectional bright-field TEM micrographs of the ZnO products grown at reactor pressures of 1, 3, and 5 Torr, respectively. The insets of (a) and (c) show the top view SEM images of the ZnO islands grown for 60 s at 1 and 5 Torr, respectively. The insets of (d), (e), and (f) show the selected area DPs (SADPs) from the ZnO/sapphire interface for reactor pressures of 1, 3, and 5 Torr, respectively.

[a)]Author to whom correspondence should be addressed; Tel.: +82 31 290 7364, FAX: +82 31 290 7410; electronic mail: chohk@skku.edu

density of the islands was high at a low reactor pressure. The ZnO islands grown at 1 and 5 Torr for 60 s showed average widths of 19 and 47 nm, respectively.

Furthermore, to elucidate the relationship between the islands at the initial state and the final morphology of the nanorods, a detailed structural characterization was performed using TEM. The cross-sectional bright-field TEM images are shown in Figs. 1(d)–1(f). In all of the samples, an interfacial ZnO layer was observed between the nanorods and the sapphire substrate, which seemed to prohibit their direct growth in the absence of the interfacial layer. With increasing pressure, the thickness of the interfacial ZnO layer increased from 77 (sample A) to 180 nm (sample B). The variation in the thickness of the interfacial layer observed on the sapphire substrates was believed to be strongly dependent on the growth rate, which is controlled by the reactor pressure. The growth rate was high for the nanorods grown at a reactor pressure of 1 Torr, and the ZnO islands nucleated in the initial state grew preferentially along the *c*-axis orientation prior to the coalescence of the grain. On the other hand, the lower growth rate along the vertical direction observed in samples B and C resulted in the coalescence of the islands in the initial stage, which caused the formation of a large and thick interfacial layer. Thus, the formation of the broad nanorods with a low aspect ratio was attributed to the increased grain size in the interfacial layer at 3 Torr. The diffraction patterns (DPs) obtained with the beam direction of $[\bar{2}110]_{ZnO}$ from the interface region revealed that the whole structures are composed of perfect single-crystal ZnO, and the epitaxial orientation relationships between the ZnO products and sapphire substrate are ZnO (0001)‖sapphire (0001) and ZnO $(10\bar{1}0)$‖sapphire $(2\bar{1}10)$. Many defects were also observed as dark lines almost perpendicular to the ZnO/sapphire interfaces, as indicated by the arrow in Fig. 1. The distance between the defects increased with increasing reactor pressure, which may have been directly related to the size and density of the islands at the initial stage. Threading dislocations are believed to be formed during the coalescence of islands at the initial stages of heteroepitaxial growth, based on the nucleation mechanism.[10]

Figure 2(a) shows the cross-sectional high-resolution TEM (HRTEM) image along the $[2\bar{1}10]_{ZnO}$ zone axis of the ZnO/sapphire interface. The $\{01\bar{1}0\}$ PDs started at the interface and stacking faults (SFs) on the (0002) plane were observed near the interface. To enable further analysis around the PDs, the enlarged HRTEM images of regions 1 and 2 of Fig. 2(a) are presented in Figs. 2(b) and 2(c), respectively. On the right-hand side of the $\{01\bar{1}0\}$ PD (region 1), we can see a SF, which is right on the surface of the sapphire. The Burgers circuit around the PD determines the stacking disorder, and is equal to the displacement vector $\mathbf{R}_I = 1/6\langle 2\bar{2}03\rangle$, which is one of the three SF vectors of the hcp structure ($\mathbf{R}_I$ of type I, $\mathbf{R}_{II}$ of type II, and $\mathbf{R}_E$ of extrinsic fault) and has the lowest formation energy.[11] The corresponding SF changes the stacking sequence, from AB**AB**ABAB to AB**ABC**BCB. Thus, the stacking sequence of the left-hand side of the PD is ABAB···, while that of the right-hand side is changed to CBCB··· with the displacement of $\mathbf{R}_I = 1/6\langle 2\bar{2}03\rangle$, and finally forms a SMB [Fig. 2(b)]. Moreover, a second SF terminates the SMB, as shown in Figs. 2(a) (region 2) and 2(c). These results were in good agreement with the SMB model

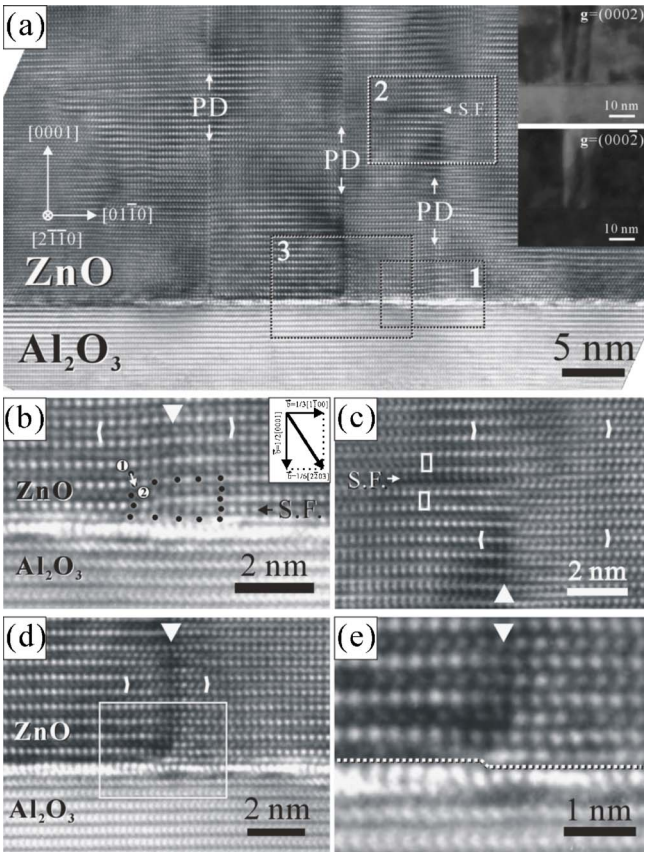

FIG. 2. (a) Cross-sectional HRTEM image along the $[2\bar{1}10]_{ZnO}$ zone axis of ZnO/sapphire interface and multiple dark field image with $g = \pm(0002)$. Enlarged HRTEM images from regions (b) 1, (c) 2, and (d) 3, marked by rectangles in (a). (e) Magnified HRTEM image of region 3 showing a step on the substrate surface. The inset of (b) shows a Burgers circuit with the starting point 1 and end point 2.

proposed by Northrup *et al.*[12] Therefore, we proposed that the coalescence of the islands having different stacking sequences in the initial stage on the sapphire substrate is responsible for the appearance of the SMBs. On the other hand, the $\{01\bar{1}0\}$ PD observed in region 3 of Fig. 2(a) has the same stacking sequence around it, as shown in Fig. 2(d), and the columnar domains appear bright with $g = (0002)$ and dark with $g = -(0002)$ in comparison with the surrounding matrix, as shown in Fig. 2(a). This characteristic corresponds to the atomic model of the IDB proposed by previous reports[12,13] and the small section inside the rectangle of Fig. 2(d) containing the PD was magnified in Fig. 2(e). The enlarged image allows us to distinguish the presence of a step on the surface of the substrate, which originated from the height difference of the surface atoms. Ruterana *et al.*[14] emphasized that IDBs are generated mostly at the surface steps, where they are shown to minimize the large misfit along the *c* axis. Therefore, the IDB formation observed in the ZnO grown on sapphire is ascribed to the inhomogeneous nature of the interface. However, since the width of inversion domains is very narrow (~10 nm) and their density is low, the effect of the polarity inversion on structural change can be ignored. In contrast with the presence of only vertically aligned PDs in sample A, inclined PDs were observed in sample B, as indicated by the arrows in Fig. 3(a). The density of the inclined PDs was increased in the interfacial layer far from the interface. The HRTEM image shows that their boundaries were

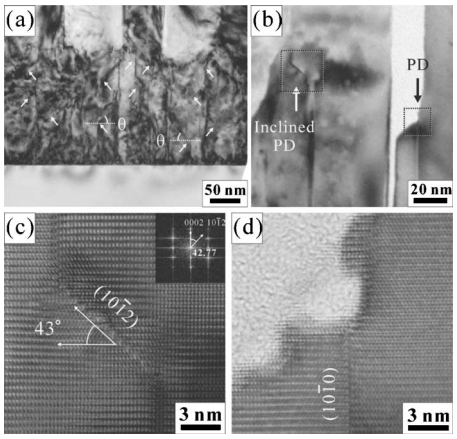

FIG. 3. (a) Cross-sectional bright-field TEM image using (0002) two-beam condition of interfacial layer grown at reactor pressure of 3 Torr. (b) Enlarged image including planar defects. HRTEM images of (c) the $(10\bar{1}2)$ inclined and (d) the $(10\bar{1}0)$ planar defects.

inclined at an angle of about 43° to the basal plane. Interestingly, these inclined PDs again turned into $\{01\bar{1}0\}$ PDs and finally formed the side face of the nanorods grown on the interface layer, as shown in Figs. 3(b) and 3(d). The fast-Fourier transformed DP of the HRTEM image obtained from the dotted rectangle in Fig. 3(b) clearly revealed that the inclined boundaries of the PDs constituted the $\{10\bar{1}2\}$ plane, as shown in the inset of Fig. 3(c).

Considering the results concerning the microstructural changes at different reactor pressures and the origin of the defects in the interfacial layers, we propose a model to explain the growth mechanism of ZnO nanorods on sapphire substrates, as demonstrated in Fig. 4. As observed from the top view SEM images, the high density islands at a reduced

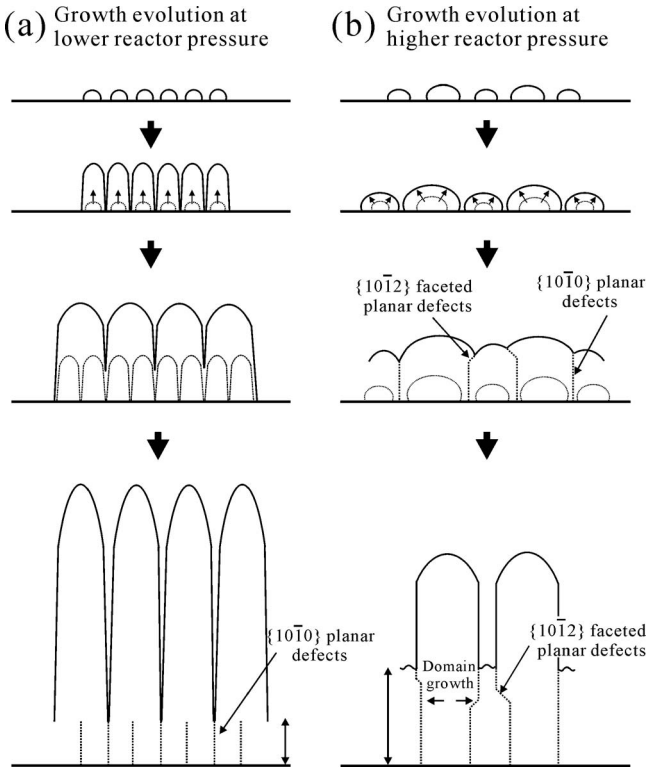

FIG. 4. Schematic model of the growth mechanism of (a) narrow and (b) broad ZnO nanorods grown with a *c* axis preferred orientation.

reactor pressure were nucleated on the sapphire substrate in the initial state and grew preferentially along the *c*-axis orientation prior to the coalescence of the grain. Their continuous growth led to the coalescence of these islands with different stacking sequences, resulting in the formation of planar boundaries between adjacent islands. These incoherent boundaries were considered to be the origin of the TDs and SMBs, as shown in the TEM results. Further growth led to the growth of the nanorods on the thin interfacial layer with the SMBs forming the side facets of the nanorods [Fig. 4(a)]. In contrast, fat nanorods with a low density and a reduced aspect ratio were grown at an increased reactor pressure due to their enhanced lateral growth. After the nucleation, the larger islands with random size coalesced and defects were also formed at the boundaries. During the coalescence process, the larger islands grew continuously or ripened at the expense of the smaller ones, thereby exhibiting "Ostwald ripening" behavior, which caused the inclination of the vertical $\{01\bar{1}0\}$ PDs. After the complete coalescence of the islands, nanorod growth commenced and the thick interfacial layer with the large grains was formed [Fig. 4(b)].

In summary, we demonstrated the initial growth behavior and resulting microstructural properties of ZnO products heteroepitaxially grown by MOCVD on sapphire substrates at different reactor pressures. Well-aligned slim ZnO nanorods with a high aspect ratio were grown at a lower reactor pressure, whereas less well-aligned fat ZnO nanorods with a low aspect ratio were grown at a higher reactor pressure. The microstructural investigations revealed the presence of PDs such as SMBs and IDBs in the interfacial layer. Based on the microstructural changes and origin of the defects in the interfacial layers, a model was proposed to explain the growth mechanism of ZnO nanorods on sapphire substrates.

This work was supported by the Korea Research Foundation Grant funded by the Korean Government (MOEHRD) (KRF-2006-311-D00143) and by Grant No. R01-2006-000-10027-0 from the Basic Research Program of the KOSEF.

[1]Z. L. Wang, Adv. Mater. (Weinheim, Ger.) **12**, 1295 (2000).
[2]J. Hu, T. W. Odom, and C. M. Lieber, Acc. Chem. Res. **32**, 435 (1999).
[3]Z. Qui, K. S. Wong, M. Wu, W. Lin, and H. Xu, Appl. Phys. Lett. **84**, 2739 (2004).
[4]Q. Wan, Q. H. Li, Y. J. Chen, T. H. Wang, X. L. He, J. P. Li, and C. L. Lin, Appl. Phys. Lett. **84**, 3654 (2004).
[5]Q. H. Li, Q. Wan, Y. X. Liang, and T. W. Wang, Appl. Phys. Lett. **84**, 4556 (2004).
[6]M. H. Huang, S. Mao, H. Feick, H. Yan, Y. Wu, H. Kind, E. Weber, R. Russo, and P. Yang, Science **292**, 1897 (2001).
[7]S. Fan, M. G. Chapline, N. R. Franklin, T. W. Tombler, A. M. Cassell, and H. Dai, Science **283**, 512 (1999).
[8]X. H. Wu, L. M. Brown, D. Kapolnek, S. Keller, B. Keller, S. P. DenBaars, and J. S. Specka, J. Appl. Phys. **80**, 3228 (1996).
[9]J. L. Rouviere, M. Arlery, B. Daudin, G. Feuillet, and O. Briot, Mater. Sci. Eng., B **50**, 61 (1997).
[10]I. Akasaki, H. Amano, Y. Koide, K. Hiramatsu, and N. Sawaki, J. Cryst. Growth **98**, 209 (1989).
[11]J. E. Northrup, L. T. Romano, in *Properties, Processing and Applications of Gallium Nitride and Related Semiconductors*, Emis Datereviews Series No. 23, edited by J. H. Edgar, S. Strite, I. Akasaki, H. Amano, and C. Wetzel, (INSPEC/IEE, London, 1999), pp. 213–220.
[12]J. E. Northrup, J. Neugebauer, and L. T. Romano, Phys. Rev. Lett. **77**, 103 (1996).
[13]L. T. Romanoa, J. E. Northrup, and M. A. O'Keefe, Appl. Phys. Lett. **69**, 2394 (1996).
[14]P. Ruterana, V. Potin, B. Barbaray, and G. Nouet, Philos. Mag. A **80**, 937 (2000).